Temperature and angular dependence of the anisotropic magnetoresistance in epitaxial Fe films

R. P. van Gorkom,* J. Caro, T. M. Klapwijk, and S. Radelaar

Department of Applied Physics and Delft Institute of Microelectronics and Submicrontechnology, Delft University of Technology, Lorentzweg 1, 2628 CJ Delft, The Netherlands

We perform detailed temperature dependent measurements of the magnetoresistance (MR) and its angular dependence of epitaxial Fe (110) films. The angular dependence of the MR at $H = 10$ kOe is found to change strongly when going from $T = 4.2$ K to $T = 230$ K. We analyze the data on the basis of Döring's equation. Second- and fourth-order angular dependent terms are found to be of equal importance, indicating strong deviations of the MR from a simple $\cos^2 \phi$ dependence. One of the MR components is the ordinary or Lorentz magnetoresistance, which is strong at low temperatures and becomes smaller at higher temperatures, due to the reduction of the mean free path. By subtracting the ordinary magnetoresistance from the MR data we obtain the anisotropic magnetoresistance. We decompose the temperature dependent anisotropic magnetoresistance in the temperature dependent k constants of Döring's equation. These constants show a reduction between $T = 20$ K and $T = 100$ K, which reflects the observed decrease of the anisotropic magnetoresistance. We present arguments that the temperature dependence of the anisotropic magnetoresistance is most likely due to the change from defect-dominated scattering to phonon-dominated scattering, each of which has its own anisotropic magnetoresistance.

I. INTRODUCTION

The discovery of the giant magnetoresistance (GMR) of magnetic multilayers[1] has stimulated a strong interest in the properties of ferromagnetic films in general,[2] in particular, in the magnetoresistance (MR) of such films. In spite of extensive experimental work, the MR of a one-layer film is only partly understood. The problem is that the MR of such a thin film is built up from various contributions of different physical origin. The most important contributions are the anisotropic magnetoresistance (AMR) and ordinary (Lorentz) magnetoresistance (OMR).

The AMR is caused by the spin-orbit interaction, which induces mixing of spin-up and spin-down d states.[3-5] This mixing depends on the magnetization direction, i.e., the direction of the net spin density. Therefore, the magnetization direction determines the density of unoccupied d states at the Fermi level. This gives rise to a magnetization-direction dependent s-d scattering rate, which dominates the resistance in ferromagnets. As a result, the resistivity of a saturated polycrystalline sample is determined by the angle ϕ between the electrical current $\mathbf{I}$ and the magnetization $\mathbf{M}$:[3] $\rho = \rho_\perp + (\rho_\parallel - \rho_\perp)\cos^2 \phi$. Here $\rho_\parallel$ is the resistivity for $\mathbf{I} \parallel \mathbf{M}$ and $\rho_\perp$ is the resistivity for $\mathbf{I} \perp \mathbf{M}$. Usually $\rho_\parallel$ exceeds $\rho_\perp$. The $\cos^2 \phi$ dependence results from averaging over all crystal orientations.[3] In bulk alloys at low temperature, where only impurity scattering occurs, the magnitude of the AMR effect can be several tens of percents, e.g., 20% for NiFe at $T = 20$ K.[3] Phonon scattering in bulk alloys brings the magnitude down to about 5% at room temperature. In thin films the AMR is further reduced to a few percent due to surface scattering and additional structural defects. When the field is swept through the range $-H_{sat} < H < H_{sat}$ (H_{sat} is the saturation field) either a resistance maximum or minimum is found, depending on the angle ϕ. This reflects the evolution of a multidomain state to a single domain state.

The OMR is due to the Lorentz force, which bends the conduction electrons away from the electric field direction, increasing the resistivity of a conductor with increasing magnetic field.[6] The magnitude of the OMR is proportional to the square of the magnetic induction $\mathbf{B}$, where $\mathbf{B} = \mathbf{H} + 4\pi\mathbf{M}$. Like the AMR, the OMR of a ferromagnet shows a maximum or minimum around $H = 0$ Oe, because the magnetization changes direction around $H = 0$ Oe. However, since for the OMR $\rho_\perp > \rho_\parallel$, the ϕ dependence is opposite to that of the AMR. The OMR does not reach saturation at H_{sat}, contrary to the AMR, but always has a positive slope for $|H| > H_{sat}$. The amplitude of the OMR increases with increasing electron mean free path and can be comparable to the AMR, which leads to an entanglement problem. The magnitude and angular dependence of both the AMR and OMR depend on the temperature and on the purity and structure of the material. To disentangle these contributions, a careful study of the angular, as well as the temperature dependence of the MR, is necessary.

In single crystals, contrary to polycrystals, averaging of the AMR resistivity over all crystal orientations is absent. Already in 1938, Döring[7] showed experimentally that bulk Ni single crystals have a much more complicated MR than polycrystalline samples. The angular dependence did not obey a behavior involving only the relative orientation of current and magnetization. Instead, the orientation of both current and magnetization with respect to the crystal axes had to be taken into account. Later, measurements on single crystal Fe rods and whiskers confirmed Döring's results.[8-11] The thin film equivalent of a bulk single crystal is the epitaxial film, which can be grown on a suitable substrate with modern deposition techniques. MR measurements on epitaxial ferromagnetic films also indicate deviations from the simple $\cos^2 \phi$ behavior and suggest that the directions of both the current and magnetization with respect to the crystal axes are important, as for bulk single crystals.[12-19] However,
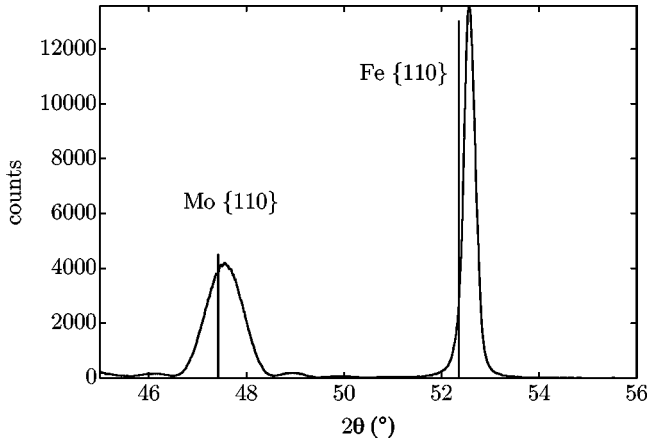
FIG. 1. θ-2θ scan of Mo(10 nm)/Fe(100 nm) deposited on $(11\bar{2}0)$ sapphire, using Co $K\alpha$ radiation ($\lambda = 1.78897$ Å). The vertical lines denote the peak positions for unstrained bulk materials.

FIG. 2. Φ scans for the {110} Fe peaks and the Al_2O_3 {11$\bar{2}$3} peaks with $\theta = 22.4°$ and $\chi = 60°$ (full line, left-hand side axis) $\theta = 21.7°$ and $\xi = 28.7°$ (dashed line, right hand side axis), respectively, using Cu $K\alpha$ radiation ($\lambda = 1.542$ Å).

the data and analysis are rather limited.

We investigate the MR of high purity epitaxial Fe films as a function of the in-plane magnetization direction with respect to the crystal orientation. This is done for two current directions and over a broad temperature range. We will demonstrate a strong dependence of the MR on the current direction, magnetization direction, and temperature. In particular, from detailed MR measurements as a function of the angle between the magnetization and crystal axes, we show how the MR deviates from the polycystalline $\cos^2 \phi$ behavior. We analyze the data with the theoretical description based on the symmetry of the crystal,[7] which yields the temperature dependence of the Döring constants. At low temperatures ($T \lesssim 50$ K) AMR and OMR are of comparable magnitude. At higher temperatures the AMR dominates the OMR. We interpret the temperature dependence of the MR contributions on the basis of the change of dominant electron-scattering mechanism. Our results expand on previous experimental results.[12–19]

II. EPITAXIAL Fe FILMS

Epitaxial Fe films are grown in a VG-V80M UHV e-gun evaporator with base pressure 2×10^{-11} mbar, using the recipe of Clemens *et al.*[20] Substrates are $6 \times 6 \times 0.5$ mm^3 pieces of $(11\bar{2}0)$ sapphire, i.e., hexagonal (rhombohedral) Al_2O_3, on top of which a 10 nm bcc Mo seed layer is grown at $T = 923$ K at a rate of 0.02 nm/s. The bcc Fe layer is deposited at $T = 473$ K with a thickness of 100 nm and at a rate of 0.07 nm/s. The purity of the Fe granules used for the melt is at least 99.95%. The pressure during evaporation of Fe is approximately 1×10^{-10} mbar.

We use x-ray diffraction to characterize our samples, applying both θ-2θ scans and Φ scans. In Fig. 1 we give an example of a θ-2θ scan in the normal geometry, where the plane from which θ is measured is the plane of the film, i.e., we are looking at the x rays diffracted from atomic planes parallel to the surface. Both for the Mo layer and the Fe layer strong and sharp {110} peaks are present, which are shifted with respect to the peak positions of the unstrained bulk
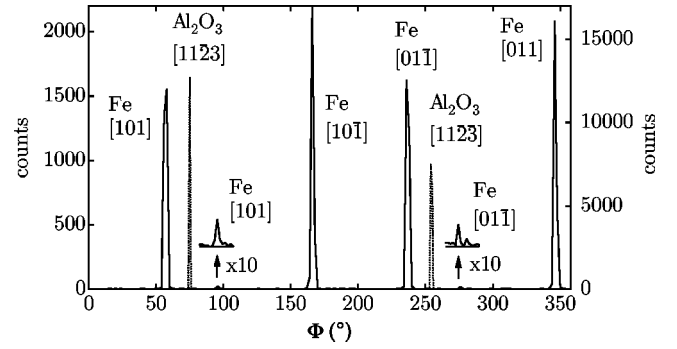
materials, represented by the vertical lines in the figure. The Mo peak has satellites due to the finite thickness of the layer, indicating a uniform layer thickness, and therefore a flat Mo/Fe interface.

Figure 2 shows two Φ scans. In a Φ scan, the sample is rotated about the normal to the layers. The geometry of a Φ scan differs from that of a normal θ-2θ scan, such as in Fig. 1, in that the sample is tilted through an angle χ. The angles θ and 2θ are set to the expected Bragg peaks. Therefore, the plane from which θ is measured is no longer parallel with the plane of the film, i.e., we are investigating the stacking of atomic planes at an angle χ with respect to the plane of the film. This reveals the texture of the films. Figure 2 shows an example of two Φ scans, adjusted for the {110} Fe peaks ($\theta = 22.4°$, $\chi = 60°$, full line, left-hand-side axis) and the {11$\bar{2}$3} Al_2O_3 peaks ($\theta = 21.7°$, $\chi = 28.7°$, dashed line, right-hand-side axis), respectively. Analysis of the scans leads to designation of the peaks, as shown in the figure, and indicates that we have a close to single-crystalline (110) epitaxial Fe layer, with the in-plane $[1\bar{1}1]$ direction aligned with the [0001] direction of the Al_2O_3. The same holds for Mo, as deduced from the relevant Φ scan. The weak Fe peaks correspond to a small Fe fraction ($\approx 0.3\%$) which has the $[1\bar{1}\bar{1}]$ direction aligned with the [0001] direction of the Al_2O_3.

The strain in the Fe layer can be calculated from the position of the Bragg peaks. For the [110] direction this is found to be (-0.40 ± 0.05)% (compressive). For the [101] and $[10\bar{1}]$ directions the strain can be determined by tilting the sample to $\chi = 60°$, Φ to the angle determined from the Φ scan, and by scanning θ and 2θ over the Bragg peak. The result is a strain of (0.11 ± 0.05)% (tensile) for the [101] direction and (0.15 ± 0.05)% (tensile) for the $[10\bar{1}]$ direction. Therefore, if we take the principal axes along the $[1\bar{1}1]$, $[1\bar{1}\bar{2}]$, and [110] directions of the Fe (the [0001], $[1\bar{1}00]$, and $[11\bar{2}0]$ of the sapphire), then within the experimental accuracy $\epsilon_{11} = \epsilon_{22} = (0.003 \pm 0.001)$ and $\epsilon_{33} = (-0.0040 \pm 0.0005)$. These strains are consistent with the Poisson ratio $\nu(\text{Fe}) \approx 0.3$.[21] The cubic symmetry of the Fe lattice is thus broken due to the slight strain anisotropy.

Thus we have well characterized epitaxial Fe films, which allow accurate measurements of the dependence of the resistance on the electrical current direction and the magnetization direction with respect to the crystal axes. These epitaxial films have the standard crystalline anisotropy of bcc Fe, which has the easy axes of magnetization along the $\langle 100 \rangle$ directions. Taking into account the magnetostatic energy for the thin film geometry, the (in-plane) [001] direction is the single easy axis of the films.

From these films we make strips with different in-plane crystal direction by mechanical scratching approximately 1.5 mm wide and 6 mm long areas. Four wires are bonded to each strip, thus allowing a four-point resistance measurement. The positioning of the wires is such that a homogeneous current density is generated between the voltage probes, along the length direction of the strip. The resistance of a strip is typically 1 Ω at room temperature. We will discuss in detail the results obtained on two samples with different angles between the electrical current direction and the [001] direction, samples A and B. More samples have been measured, showing similar results. In sample A, the [001] direction and the current direction make an angle of $\theta = -20° \pm 3°$, as shown in the inset of Fig. 3. This angle was chosen because it is not one of the high symmetry directions, in which a more regular behavior may be expected. The resistance ratio between $T = 300$ K and $T = 4.2$ K (the residual resistance ratio) is equal to 16. For sample B, the current flows approximately parallel ($\theta = 0° \pm 3°$) to the [001] direction. It has a residual resistance ratio of 11.5.

III. MAGNETORESISTANCE MEASUREMENTS

Magnetoresistance measurements are done between 4.2 K and 230 K in an He flow cryostat equipped with a superconducting magnet and *in situ* sample rotation capabilities. The resistance of the samples is measured with a dc current of 50 mA, which is low enough to prevent significant heating. In Fig. 3 we show magnetoresistance traces $(R - R_{H=0})/R_{H=0}$ for sample A, measured for several magnetic field directions, at 4.2 and 80 K. Each trace is measured in field sweeps from $H = 10$ to -10 kOe and from $H = -10$ to 10 kOe. Figure 3 shows the hysteresis for certain angles between the current and magnetization direction. The $\phi = -75°$ curve in Fig. 3(b) shows a pronounced hysteresis at $H = 0.64$ kOe. For the MR curves for $\phi = -60°$ and $\phi = 0°$ in Figs. 3(a) and 3(b), respectively, hysteresis is virtually absent. This is representative for the other angles as well. Therefore, for those angles only a single trace is shown. The curves with $\phi = 90°$ and $\phi = -90°$ coincide, which demonstrates the accuracy of the rotational mechanism, because rotating by 180° is equivalent to reversing the magnetic field direction and the MR is symmetric with reversal of the magnetic field. In both Figs. 3(a) and 3(b) a complicated angular dependence of the MR traces is clearly present, which strongly depends on temperature.

For all traces, the resistance at $H = 0$ kOe is independent of the angle of the previously applied magnetic field. Apparently the magnetization always rotates into the easy magnetization direction at $H = 0$ kOe. The magnetization direction in the low magnetic field region ($H \lesssim 3$ kOe) is determined
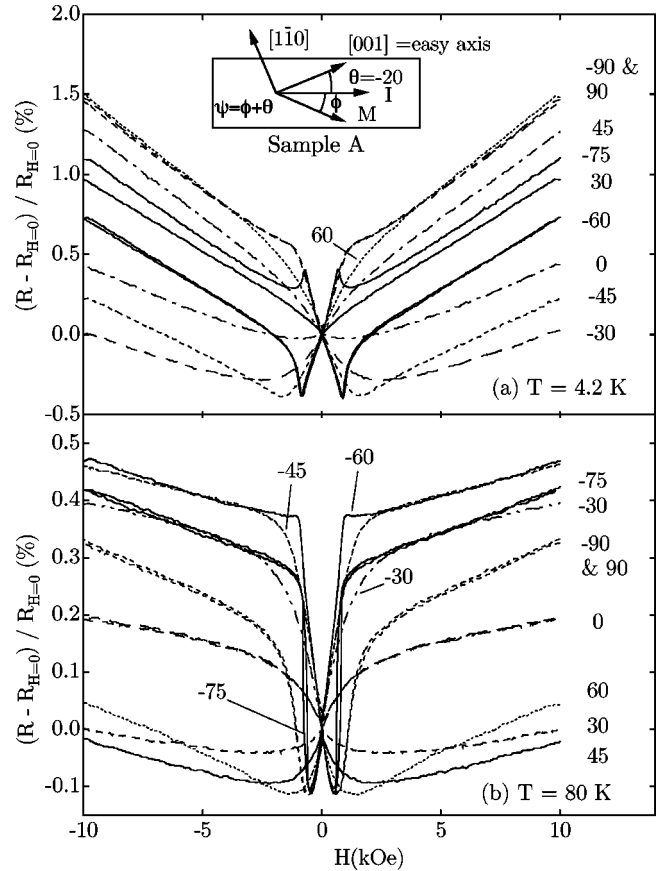

FIG. 3. Magnetoresistance traces for sample A at different angles of the applied magnetic field with respect to the electrical current at (a) $T = 4.2$ K and (b) $T = 80$ K. The current flows at an angle of 20° with the [001] axis (the easy axis), as shown in the inset. **M** is the magnetization, **I** is the current, $\theta = -20°$ is the angle between the current and the [001] direction, ϕ is the angle between the current and magnetization, and ψ is the angle between the magnetization and the [001] direction.

by the competition between the torques on the magnetization exerted by the external magnetic field and crystalline anisotropy field. With increasing field strength the magnetization direction rotates towards the field direction. The rotation either causes an increase or decrease in the resistance, depending on the angle of the field with respect to the electrical current direction. At approximately $|H| = 0.5$ kOe, in certain curves a nonmonotonous behavior is present. At $T = 4.2$ K, maxima are present in the $\phi = -75°$ curve and minima are present in the $\phi = -60°$, $-45°$, $-30°$ and $0°$ curves. Minima are also present in the $T = 80$ K curves, for $\phi = -75°$, $-90°$, $90°$, $60°$, $45°$, and $30°$. It is likely that the maxima and minima we measure in our samples arise as follows. First, when the magnetization points somewhere in between the easy magnetization direction and applied magnetic field direction, the resistance can go through either a maximum or a minimum as a function of the angle. This is the case for the $\phi = -75°$, $-60°$, and $-45°$ curves at $T = 4.2$ K, and $\phi = -75°$, $-90°$, $90°$, $60°$ curves at $T = 80$ K. Second, when the magnetization initially rotates towards the magnetic field direction, the resistivity can decrease. How-
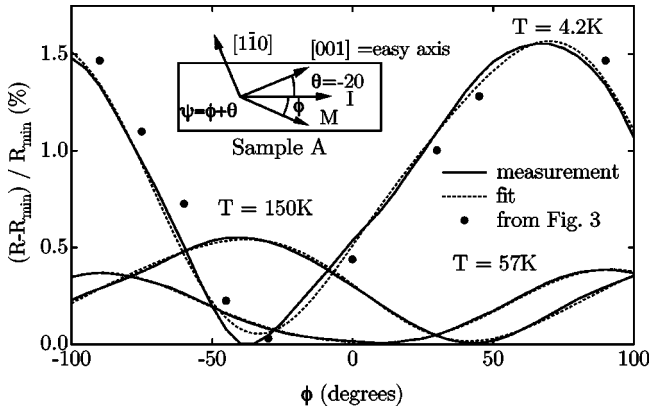
FIG. 4. The magnetoresistance of sample A at $H=10$ kOe as a function of the angle between the applied magnetic field and the electrical current at (a) $T=4.2$ K, (b) $T=57$ K, and (c) $T=150$ K. The measurement geometry is as in Fig. 3.

ever, the combined effect of the negative AMR and positive OMR results in the observed minimum for $\phi=-30°$ and $0°$ curves at $T=4.2$ K, and $\phi=45°$ and $30°$ curves at $T=80$ K. We note that this behavior is strongly different from the behavior of polycrystalline samples, which show a single minimum and a maximum around $H=0$ Oe for the magnetic field parallel and perpendicular to the current direction, respectively.

At the high field region ($H>H_{sat}\approx3$ kOe; H_{sat} is the saturation magnetic field) a monotonous increase in resistance with increasing magnetic field is observed for all MR curves, which is due to the OMR effect. The magnetization is saturated in this region. In analyzing the angular dependence of the resistance at 10 kOe, we see that also a complicated angular dependence is present, e.g., in Fig. 3(a) the $\phi=-90°$ and $90°$ measurements are the topmost, while the $\phi=-30°$ measurement is the bottom curve. In Fig. 3(b) the $\phi=-60°$ measurement is the topmost curves, while the $\phi=45°$ measurement is the bottom curve. The resistance at 10 kOe is plotted versus ϕ in Fig. 4, marked by the solid dots. Clearly, the angular dependence is not a simple $\cos^2\phi$, i.e., the dependence differs from the angular dependence of the AMR effect of a polycrystalline material.

At high fields domain-wall magnetoresistance is not present, because the magnetization of the sample is saturated. This leaves the AMR and OMR of a saturated sample as the remaining contributions to the MR. Therefore, to disentangle these contributions it is advantageous to focus on the angular dependence of the MR at high field, for which we choose 10 kOe.

In Fig. 4 we give examples of the relative resistance change $(R-R_{min})/R_{min}$ of sample A as a function of the angle between the current and magnetization, for $T=4.2$ K, $T=57$ K, and $T=150$ K. R_{min} is the minimum resistance. The resistance is measured by stepping ϕ from $-100°$ to $100°$ in steps of $5°$. The reverse curves from $\phi=100°$ to $-100°$ are also measured in order to test the reproducibility, which is good, except for a small temperature drift at higher temperatures ($\Delta R/R$ due to the temperature drift is 0.02% for $T=230$ K and $\Delta R/R<0.003\%$ for $T<155$ K). Figure 4
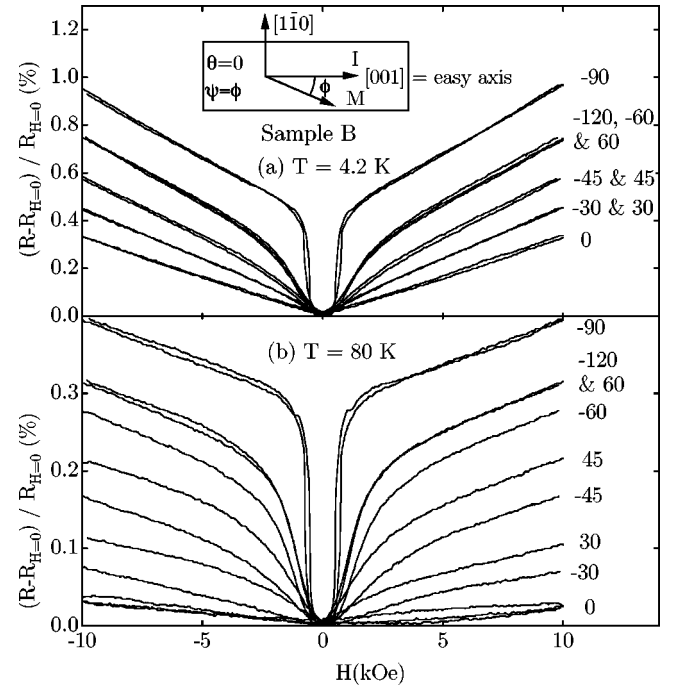

FIG. 5. Magnetoresistance traces for sample B at different angles of the applied magnetic field with respect to the electrical current at (a) $T=4.2$ K and (b) $T=80$ K. The current flows along the [001] axis (the easy axis), as shown in the inset. **M** is the magnetization, **I** is the current, $\theta=0°$ is the angle between the current and the [001] direction, ϕ is the angle between the current and magnetization, and $\psi(=\phi)$ is the angle between the magnetization and the [001] direction.

shows that the fixed field measurement as a function of the angle agrees well with the measurements in Fig. 3. A small offset angle of $\approx4°$ is present, which is the experimental alignment error. Figure 4 confirms that the curves are not symmetric around $\phi=0°$ and that the minimum shifts with temperature. Furthermore, the shape is not a simple $\cos^2\phi$ dependence. For example, in the $T=4.2$ K measurement, the minimum of the curve is sharper than the maximum.

MR measurements of sample B are shown in Fig. 5. Also for this sample, at zero field all curves meet in one point, as with the previous sample, but the angular dependence is now much simpler. The resistance as a function of the angle between the current direction and the magnetization direction at $H=10$ kOe is shown in Fig. 6. Curves at higher temperatures are shown compared to Fig. 4, in order to show the change to a nonsinusoidal curve at higher temperatures more clearly. The curves are almost symmetric around $\phi=0°$. For $T=80$ K and $T=184$ K a small asymmetry is present. We observe that also for this sample, the resistance as a function of the angle is not a $\cos^2\phi$, as is the case for a polycrystalline sample. This is most clearly visible at $T=184$ K, where an extra minimum is present at about $\phi=90°$. The other two curves at $T=80$ K and $T=4.2$ K do resemble a $\sin^2\phi$, but the curves show a much sharper maximum than minimum, indicating that again it is not a perfect sinusoidal dependence.

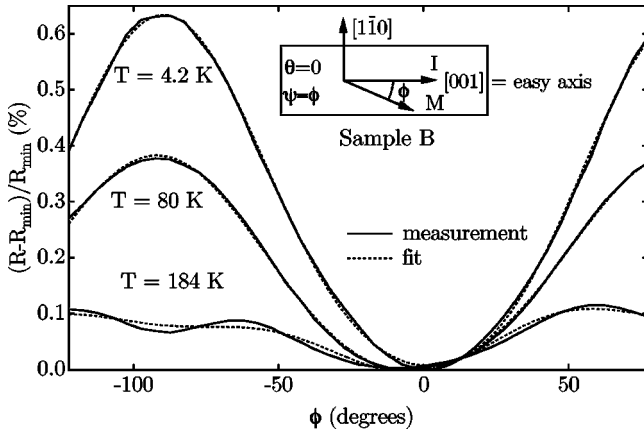In the next section we will analyze the angular depen-

FIG. 6. Magnetoresistance of sample B at $H=10$ kOe as a function of the angle between the applied magnetic field and the current at (a) $T=4.2$ K, (b) $T=80$ K, and (c) $T=184$ K. The measurement geometry is as in Fig. 5.

dence of the resistance on the basis of AMR and OMR.

IV. ANALYSIS AND DISCUSSION

We analyze our data with the expression of Döring[7] for the resistivity, which is based on the symmetry of the crystal. He assumed that the electric field components E_1, E_2, and E_3 along the cubic directions are linear functions of the components j_1, j_2, and j_3 of the electrical current density: $E_i = \Sigma_{k=1}^{3} w_{ik} j_k$. Here w_{ik} are the magnetization-direction dependent components of the magnetoresistivity tensor, which describes all ohmic MR effects, including AMR and OMR. The resistivity can be written as $\rho = \Sigma_{i,k=1}^{3} w_{ik} \beta_i \beta_k$, where β_1, β_2, and β_3 are the direction cosines of the electrical current with respect to the cubic axes. The components w_{ik} can be rewritten using the symmetry of a cubic crystal. This yields for the relative change in resistivity for arbitrary current and magnetization directions:[7,22]

$$
\frac{\rho - \rho^*}{\rho^*} = k_1 \left(\alpha_1^2 \beta_1^2 + \alpha_2^2 \beta_2^2 + \alpha_3^2 \beta_3^2 - \frac{1}{3} \right)
$$

$$
+ 2k_2 (\alpha_1 \alpha_2 \beta_1 \beta_2 + \alpha_2 \alpha_3 \beta_2 \beta_3 + \alpha_3 \alpha_1 \beta_3 \beta_1)
$$

$$
+ k_3 s + k_4 \left(\alpha_1^4 \beta_1^2 + \alpha_2^4 \beta_2^2 + \alpha_3^4 \beta_3^2 + \frac{2}{3} s - \frac{1}{3} \right)
$$

$$
+ 2k_5 (\alpha_1 \alpha_2 \alpha_3^2 \beta_1 \beta_2 + \alpha_2 \alpha_3 \alpha_1^2 \beta_2 \beta_3
$$

$$
+ \alpha_3 \alpha_1 \alpha_2^2 \beta_3 \beta_1), \tag{1}
$$

where ρ^* is the average resistivity of a hypothetical multidomain sample with equal volume fractions with the magnetization pointing along a {100} direction, k_1, k_2, k_3, k_4, and k_5 are temperature dependent constants, α_1, α_2, and α_3 are the direction cosines of the magnetization direction with respect to the cubic axes and $s = \alpha_1^2 \alpha_2^2 + \alpha_2^2 \alpha_3^2 + \alpha_3^2 \alpha_1^2$. The local magnetization direction should be used if the sample is in a multidomain state. Equation (1) then describes the local change in resistivity. Equation (1) is an expansion based on

the symmetry of the crystal. Therefore, it is hard to directly relate the k constants to physical properties such as the spin-orbit interaction. The relation of the k constants with the underlying physics should follow from first principle AMR models, but that is beyond the scope of this article.

For our purpose, we adapt Eq. (1) to the specific geometry of our (110) films, using $\alpha_1 = -\alpha_2 = (1/\sqrt{2})\sin \psi$, $\alpha_3 = \cos \psi$, $\beta_1 = -\beta_2 = (1/\sqrt{2})\sin \theta$, and $\beta_3 = \cos \theta$. Here ψ is the angle between the magnetization and the [001] direction and θ is the angle between the electrical current and the [001] direction (see inset Fig. 3). This leads to four independent terms in Eq. (1):

$$
\frac{\rho - \rho^*}{\rho^*} - \delta = C_1 \cos^2 \psi + C_2 \cos^4 \psi + C_3 \cos \psi \sin \psi
$$

$$
+ C_4 \cos \psi \sin^3 \psi, \tag{2}
$$

where

$$
C_1 = k_1 \left(\cos^2 \theta - \frac{1}{2} \sin^2 \theta \right) - k_2 \frac{1}{2} \sin^2 \theta
$$

$$
+ k_3 \frac{1}{2} + k_4 \left(\frac{1}{3} - \frac{1}{2} \sin^2 \theta \right) + k_5 \frac{1}{2} \sin^2 \theta, \tag{3}
$$

$$
C_2 = -k_3 \frac{3}{4} + k_4 \left(\cos^2 \theta + \frac{1}{4} \sin^2 \theta - \frac{1}{2} \right) - k_5 \frac{1}{2} \sin^2 \theta, \tag{4}
$$

$$
C_3 = 2k_2 \cos \theta \sin \theta, \tag{5}
$$

$$
C_4 = k_5 \cos \theta \sin \theta, \tag{6}
$$

and

$$
\delta = k_1 \left(\frac{1}{2} \sin^2 \theta - \frac{1}{3} \right) + k_2 \frac{1}{2} \sin^2 \theta + k_3 \frac{1}{4} + k_4 \left(\frac{1}{4} \sin^2 \theta - \frac{1}{6} \right). \tag{7}
$$

A linear term in ψ is added to Eq. (2) to take into account the small temperature drift in our measurements at high temperatures (while stepping through the range of angles [$\phi_{\text{start}}, \phi_{\text{end}}$] the resistance drifts linearly in time). A linear term is orthogonal to the other terms, so that it does not influence these in principle, but helps to correctly weigh each measurement point. It is not possible to determine both ρ^* and δ from the measurements. Therefore, we use [$\rho - \rho^*(1 + \delta)$]$/\rho^* \approx (R - R_0)/R_0$, which introduces a negligible error ($\approx 1\%$) compared to the other errors in the C coefficients.

We analyze the resistance versus angle data with Eq. (2) for measurements at up to 13 different temperatures in the range 4.2–220 K for each sample, using $\psi = \phi + \theta$. In the analysis, the value of the coefficients C_1, C_2, C_3, and C_4 results from a fitting procedure. In general, good agreement between the experimental data and Eq. (2) is obtained, as exemplified by the fit results in Figs. (4) and (6). The temperature dependence of the C coefficients is plotted in Figs. 7 and 8, where the error bars reflect the different fit results obtained for curves measured with opposite angle-step direction at each temperature. The following general observations
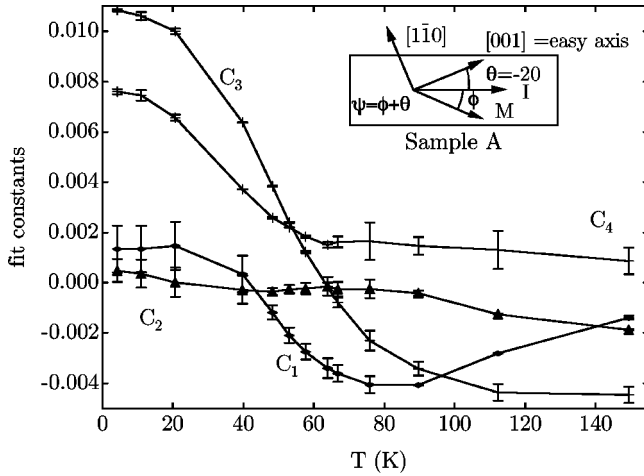
FIG. 7. Temperature dependence of the fit coeficients C_1, C_2, C_3, and C_4, obtained by fitting Eq. (2) to the data from sample A.

can be made: (1) either C_2 or C_4 is significantly different from zero, and can be comparable to C_1 and C_3, at most temperatures. This is in contrast to polycrystalline samples, for which C_2 and C_4 are zero for all temperatures.[3] (2) There is no temperature where all four coefficients are zero simultaneously, i.e., there is no ''compensation temperature,'' where the resistivity is independent of the magnetization direction. (3) All coefficients except C_4 in Fig. 7 change sign as a function of temperature. (4) Most coefficients have a maximum gradient at $T \approx 60$ K. (5) For sample B (see Fig. 8), C_3 and C_4 are very close to zero. This agrees with Eqs. (5) and (6), which indicate that $C_3 = C_4 = 0$ for $\theta = 0°$. Deviations from zero relate to the uncertainty in θ ($\pm 3°$) and/or to the nonperfect texture of the sample.

From the C coefficients in Figs. 7 and 8, we calculate the k constants of Eq. (1). We combine the data from both figures because the data from only one sample are insufficient to determine the five k constants. However, due to its higher residual resistance ratio, samples A has a larger OMR at low temperatures than sample B, as can be seen from the slopes
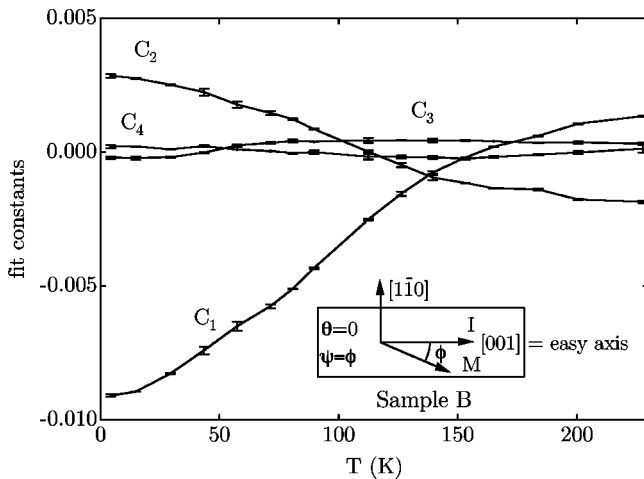

FIG. 8. Temperature dependence of the fit coeficient C_1, C_2, C_3, and C_4, obtained by fitting Eq. (2) to the data from sample B.

of the MR at high fields in Figs. 3 and 5. Therefore, to combine the two data sets, we need to subtract the OMR contribution from the C coefficients of sample A and B. We estimate the OMR from[23] $(\Delta\rho/\rho)_{OMR} \approx (eB_\perp \tau/m^*)^2$, which is the solution of the Boltzmann transport equation up to the second order in the magnetic induction in the limit $(eB_\perp \tau/m)^2 \ll 1$. Here τ is the momentum relaxation time, e is the electron charge, m^* is the effective electron mass, and $B_\perp = |\mathbf{H} + 4\pi\mathbf{M}|\sin\phi$ is the component of the magnetic field perpendicular to the current direction. Combining the above equation for the OMR with the resistivity $\rho = m/(ne^2\tau)$, we find that $(\Delta\rho/\rho)_{OMR} = \kappa(\rho^2_{300 K}/\rho^2)\sin^2\phi$. Here $\kappa = [B/(ne\rho_{300 K})]^2$ is a temperature independent constant and $\rho_{300 K}$ is the resistivity at $T = 300$ K. We estimate κ from the MR in Figs. 3 and 5 for fields above H_{sat}, where the AMR is constant. This is done by applying the expression for $(\Delta\rho/\rho)_{OMR}$ to the difference in resistance change for the parallel and perpendicular field orientations, when going from a small field (≈ 3 kOe) to a large field (≈ 10 kOe) and by taking into account the magnetization ($4\pi M = 22$ kG).[24] We find that $\kappa = (3.5 \pm 0.2) \times 10^{-5}$ at $B = 32$ kG ($H = 10$ kOe, which is the field of the angular measurements). Using $\psi = \phi + \theta$ and rewriting $\sin^2\phi$ in terms of ψ and θ, we find the coefficients without the OMR:

$$\hat{C}_1 = C_1 - \kappa \frac{\rho^2_{300 K}}{\rho^2}(\sin^2\theta - \cos^2\theta), \qquad (8)$$

$$\hat{C}_3 = C_3 + \kappa \frac{\rho^2_{300 K}}{\rho^2} 2\cos\theta\sin\theta, \qquad (9)$$

and

$$\hat{\delta} = \delta - \kappa \frac{\rho^2_{300 K}}{\rho^2}\cos^2\theta. \qquad (10)$$

We neglect the OMR contribution to C_2 and C_4, which are of order $(eB_\perp \tau/m)^4$, and therefore small compared to the AMR contribution to C_2 and C_4. Thus we have $\hat{C}_2 = C_2$ and $\hat{C}_4 = C_4$.

Using $\theta = -20°$ and $\theta = 0°$ for samples A and B, respectively, we obtain four equations from sample A [Eqs. (3)–(6)] and two equations from sample B [Eqs. (3) and (4)], which we solve for the five k constants for each temperature. The resulting temperature dependent k constants are plotted in Fig. 9. We observe that k_1, k_3, k_4 dominate at low temperatures. All constants are relatively temperature independent up to $T \approx 20$ K, where they start to change. At ≈ 85 K they bunch together in a somewhat narrow range centered around zero. Apart from k_5, all constants change sign between $T = 50$ and $T = 95$ K. Furthermore, there is no temperature where all constants are zero.

To explain the temperature dependence of the AMR contribution to the k constants, we consider three temperature dependent effects or quantities. These are excitation of thermal spin waves, lattice strain, and the dominant electron scattering mechanism.
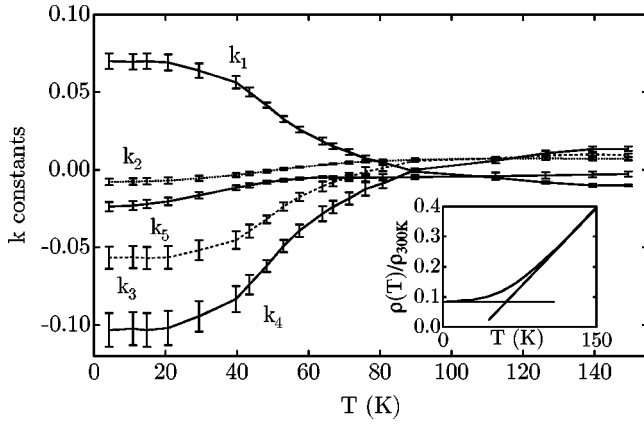
FIG. 9. The temperature dependence of k_1, k_2, k_3, k_4, and k_5 as obtained from C_1, C_2, C_3, and C_4 of Figs. 7 and 8. The inset shows the relative resistivity as a function of temperature, for sample B.

Spin waves, local and temporal oscillations of the magnetization direction, are progressively excited with increasing temperature, leading to magnetization reduction.[25] Spin waves will also cause angular averaging of the AMR resistivity because of the direction cosines α_i present in Eq. (1). This averaging is also known for the magnetocrystalline anisotropy constants which have a similar dependence on the α_i.[26] For the AMR effect, the averaging leads to effective, temperature dependent k constants. Interpreting the reduction of the AMR effect analyzed by Parker[27] in this way, one would expect a reduction of the k constants as $[M(T)]^2$. The change of the constants in Fig. 9, when replotted versus $M(T)$, is much faster than this. Actually, however, the k constants should follow different power laws of the magnetization, because each term in Eq. (1) has a different angular dependence. This is also contrary to our finding. Therefore, spin-wave averaging does not cause the observed temperature dependence.

Furthermore, the lattice strain changes due to the temperature dependent differential thermal expansion of the Fe film and substrate. This leads to, for example, a change of overlap integrals of the d wave functions, which influences the splitting of the spin-up and spin-down bands. Such a change will influence the anisotropy of the s-d scattering responsible for the AMR effect. The thermal expansion coefficients for Fe and sapphire do not go to zero where the k constants saturate ($T > 100$ K), but in fact still become larger.[28] Although the relation between the strain and the AMR is not known, this discrepancy suggests that lattice strain is not the dominant mechanism.

Finally, with increasing temperature the dominant scattering mechanism in Fe (as in many other metals) changes from electron-defect scattering to electron-phonon scattering, as established by Isshiki and Igaki.[29] Our resistivity data for samples A and B are similar to those of Ref. 29. We therefore assume that, also in our samples, a transition from electron-defect to electron-phonon scattering occurs.[30] The inset of Fig. 9 illustrates this, with an estimated transition temperature of about $T = 60$ K. Figure 9 shows that the k constants change in the same region where the scattering changes from electron-defect dominated to electron-phonon dominated, each of which has its own AMR. The gradual transition between the contributions to the AMR due to defect and phonon scattering, $[(\rho - \rho^*)/\rho]_d$ and $[(\rho - \rho^*)/\rho]_{ph}$, respectively, is given by[3,27,31]

$$\frac{\rho - \rho^*}{\rho^*} = \frac{\Delta\rho_{ph} + \Delta\rho_d}{\rho_{ph} + \rho_d} = \frac{[(\rho - \rho^*)/\rho^*]_{ph}[\rho(T) - \rho(4.2 \text{ K})] + [(\rho - \rho^*)/\rho^*]_d\rho(4.2 \text{ K})}{\rho(T)}, \tag{11}$$

where $\rho(4.2 \text{ K}) = \rho_d$ is the resistivity caused by electron-defect scattering, ρ_{ph} is the resistivity caused by electron-phonon scattering, $\rho(T) = \rho_d + \rho_{ph}(T)$, $\Delta\rho_{ph}^* = \rho_{ph}[(\rho - \rho^*)/\rho^*]_{ph}$, and $\Delta\rho_d^* = \rho_d[(\rho - \rho^*)/\rho^*]_d$. The shape of the scattering potential depends on the scattering mechanism, which will therefore influence the probabilities of s-d scattering. According to Smit,[4] $(\Delta\rho/\rho)_{ph}$ is smaller than $(\Delta\rho/\rho)_d$ because the scattering potential for electron-phonon scattering is nonspherical, as opposed to spherical for electron-defect scattering. In other words, the AMR at low temperature is larger than the AMR at high temperatures. In Fig. 9 we can see that the magnitude of the k constants indeed shows a gradual decrease in the temperature range where the transition between the two scattering mechanisms occurs. The usual way to visualize this transition for polycrystalline ferromagnets is to plot $(\rho_\parallel - \rho_\perp)/\rho$ versus $\rho(4.2 \text{ K})/\rho(T)$ (Parker plot). Because of the more complicated angular dependence of the AMR of our epitaxial Fe films, plotting the resistivity difference for these directions is rather arbitrary and does not show all information. Instead, in Fig. 10 we give a Parker plot of k constants, which shows all data. We can see that for $\rho(4.2 \text{ K})/\rho(T) < 0.60$, within the experimental accuracy, a linear dependence in present, as suggested by Eq. (11). The intercepts of the lines with the axis are the k values for phonon scattering alone.

Considering the three possible mechanisms for the reduction of the amplitude of the AMR with increasing temperature, the most likely candidate is the change from defect-dominated scattering to phonon-dominated scattering, each of which has its own AMR.

Although literature data for Fe are scarce, a comparison with published k constants is in place. Hirone and Hori[11] determined from room temperature data by Webster[9] and Shirakawa[10] for bulk single Fe crystals that $k_1 = 0.00153$, $k_2 = 0.00593$, $k_3 = 0.00194$, $k_4 = -0.00053$, and $k_5 = -0.00269$. These k values include the OMR. They are two to
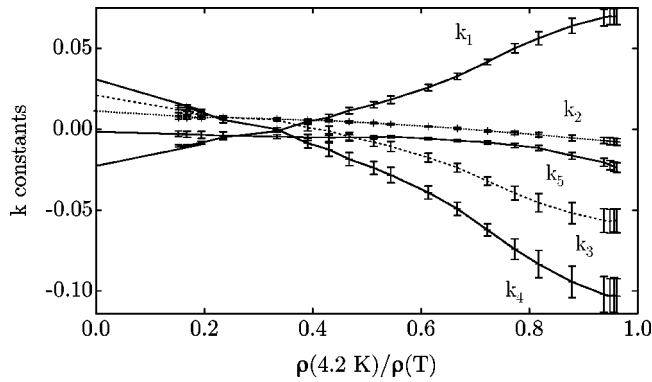
FIG. 10. Parker plot of k_1, k_2, k_3, k_4, and k_5 as obtained from the data in Fig. 9. The lines are a linear fit to the data point in the range $0.15 < \rho(4.2\,\mathrm{K})/\rho(T) < 0.60$.

ten times smaller than ours at room temperature, while k_4 in our data has the largest value followed by k_1, k_3, k_2, and finally k_5. Furthermore, the signs of k_1 and k_4 are different from those in our data. This difference cannot be explained by the OMR contribution in the data of Webster *et al.* because at room temperature the OMR is small compared to AMR. Probably, the differences result from the different nature of the samples, thin film versus bulk crystal. For example, the strain and purity in the samples can be different. To our knowledge, for Fe films literature data on k constants do not exist. The MR of several differently oriented films with several different current directions has been measured, though.[12,13,17–19] The results seem consistent with our results. However, in some papers the angular dependence was not fully taken into account, which introduces complications in the interpretation of MR data. The compensation temperature, where the resistance is independent of the magnetization direction, was reported by two articles,[17,18] but has not been found in the present work. However, up to four angles can be found in which accidentally the same resistance occurs [four angles in Fig. 6, for $0.06 < (R - R_{\min})/R_{\min} < 0.08$ at $T = 184$ K and two angles for other resistances and temperatures and also 2 angles in Fig. 4].

V. CONCLUSIONS

We have studied the MR of epitaxial Fe (110) films and its dependence on the in-plane magnetization direction as a function of temperature. The magnetization-direction dependence of the MR at $H = 10$ kOe is found to change strongly when going from $T = 4.2$ K to $T = 230$ K, as a result of a temperature dependent interplay between the ordinary and anisotropic magnetoresistance. By analyzing the data with Döring's equation it is found that second- and fourth-order angular dependent terms are found to be of equal importance, i.e., the dependence on the magnetization direction of the MR is not a simple $\cos^2\phi$. At low temperatures, the ordinary magnetoresistance, which is due to the Lorentz force, influences the MR strongly. At higher temperatures, the ordinary magnetoresistance becomes smaller, due to the reduction of the electron mean free path. Thus the anisotropic magnetoresistance, which is due to the spin-orbit interaction, becomes dominant. Considering three possible mechanisms for the reduction of the amplitude of the anisotropic magnetoresistance with increasing temperature, the most likely candidate is the change from defect-dominated scattering to phonon-dominated scattering, each of which has its own anisotropic magnetoresistance.

*Electronic address: gorkom@dimes.tudelft.nl

[1] M. N. Baibich, J. M. Broto, A. Fert, F. Nguyen, F. Petroff, P. Etienne, G. Creuzet, A. Friederich, and J. Chazelas, Phys. Rev. Lett. **61**, 2472 (1998).

[2] See, e.g., *Ultrathin Magnetic Structures II*, edited by B. Heinrich and J. A. C. Bland (Springer, Berlin, 1994).

[3] T. R. McGuire and R. I. Potter, IEEE Trans. Magn. **MAG-11**, 618 (1973).

[4] J. Smit, Physica (Amsterdam) **16**, 612 (1951).

[5] R. I. Potter, Phys. Rev. B **10**, 4626 (1974).

[6] J. P. Jan, Solid State Phys. **5**, 1 (1957).

[7] W. Döring, Ann. Phys. (Leipzig) **32**, 259 (1938).

[8] E. Fawcett and W. A. Reed, Phys. Rev. Lett. **9**, 336 (1962); W. A. Reed and E. Fawcett, Phys. Rev. **136**, A422 (1964); G. R. Taylor, A. Isin, and R. V. Coleman, *ibid.* **165**, 621 (1968); A. Isin and R. V. Coleman, *ibid.* **137**, A1609 (1965).

[9] W. L. Webster, Proc. R. Soc. London, Ser. A **A114**, 611 (1927).

[10] Y. Shirakawa, Sci. Rep. Tohoku Imp. Univ., Ser. 1 **29**, 132 (1940); **29**, 152 (1940).

[11] T. Hirone and N. Nori, Sci. Rep. Tohoku Imp. Univ., Ser. 1 **30**, 125 (1942).

[12] E. Dan Dahlberg, K. Riggs, and G. A. Prinz, J. Appl. Phys. **63**, 4270 (1988).

[13] M. Tondra, D. K. Lottis, K. T. Riggs, Y. Chen, E. D. Dahlberg, and G. A. Prinz, J. Appl. Phys. **73**, 6393 (1993).

[14] R. H. Walden and R. F. Cotellessa, J. Appl. Phys. **38**, 1335 (1967).

[15] V. A. Marsocci, J. Appl. Phys. **35**, 774 (1964); Phys. Rev. **137**, A1842 (1965).

[16] R. V. Coleman and D. C. Larson, Phys. Lett. **19**, 554 (1965).

[17] A. D. Kent, U. Ruediger, J. Yu, S. Zhang, P. M. Levy, Y. Zhong, and S. S. P. Parkin, IEEE Trans. Magn. **34**, 900 (1998); U. Ruediger, J. Yu, S. Zhang, A. D. Kent, and S. S. P. Parkin, Phys. Rev. Lett. **80**, 5639 (1998); A. D. Kent, U. Ruediger, J. Yu, L. Thomas, and S. S. P. Parkin, J. Appl. Phys. **85**, 5243 (1999).

[18] S. G. Kim, Y. Otani, K. Fukamichi, S. Yuasa, M. Nyvlt, T. Katayama, J. Magn. Magn. Mater. **198-199**, 200 (1999).

[19] P. Granberg, P. Isberg, T. Baier, B. Hjorvarsson, and P. Nordblad, J. Magn. Magn. Mater. **195**, 1 (1999).

[20] B. M. Clemens, R. Osgood, A. P. Payne, B. M. Lairson, S. Bren-

nan, R. L. White, and W. D. Nix, J. Magn. Magn. Mater. **121**, 37 (1993).

[21] This follows from $\nu = \epsilon_\perp / (\epsilon_\perp - 2\epsilon_\parallel)$, with $\epsilon_\perp$ the perpendicular strain and $\epsilon_\parallel$ the in-plane strain. This relation yields $\nu(\text{Fe}) = 0.4 \pm 0.12$, consistent with the tabulated value $\nu(\text{Fe}) \approx 0.3$ (Ref. 32).

[22] The AMR resistivity for the polycrystalline case $\rho = \rho_\parallel + \Delta\rho \cos^2(\phi)$, can be recovered by integrating Eq. (1) over all orientations of the crystal while keeping the angle between the magnetization and the current constant (Ref. 3). The assumption in this case is that the OMR is negligible for polycrystalline samples, and that therefore the complete MR is caused by the AMR effect.

[23] See, e.g., S. V. Vonsovskii, *Magnetism* (Wiley, New York, 1974).

[24] To calculate κ we use $1/(n e \rho_{300\,K}) = [\Delta R(B_2)/R_0 - \Delta R(B_1)/R_0]/[(B_2^2 - B_1^2)RRR^2]$, where $\Delta R(B)/R_0 = [R_\perp(B) - R_0]/R_0 - [R_\parallel(B) - R_0]/R_0$, $R_\parallel(B)$ is the magnetic field dependent resistance when the current and magnetic field are parallel, $R_\perp(B)$ is the magnetic field dependent resistance when the current and magnetic field are perpendicular, and RRR is the residual resistance ratio.

[25] See, e.g., A. H. Morrish, *The Physical Principles of Magnetism* (Wiley, New York, 1965).

[26] C. Zener, Phys. Rev. **96**, 1335 (1954); R. Brenner, *ibid.* **107**, 1539 (1957); W. J. Carr, Jr., J. Appl. Phys. **29**, 436 (1958).

[27] R. Parker, Proc. Phys. Soc., London, Sect. A **64**, 447 (1951); Proc. Phys. Soc. London, Sect. B **64**, 930 (1951); **65**, 616 (1952).

[28] R. K. Kirby, T. A. Hahn, and B. D. Rothrock, *American Institute of Physics Handbook*, 3rd ed., edited by D. E. Gray (McGraw-Hill, New York, 1972).

[29] M. Isshiki and K. Igaki, Trans. Jpn. Inst. Met. **19**, 431 (1978).

[30] At low temperatures surface scattering will contribute to the total scattering in the samples. Electron-defect scattering is meant to include electron-surface scattering.

[31] L. Berger and S. A. Friedberg, Phys. Rev. **165**, 670 (1968); L. Berger, P. P. Freitas, J. D. Warner, and J. E. Schmidt, J. Appl. Phys. **64**, 5459 (1988); P. P. Freitas, L. Berger, and J. F. Silvain, *ibid.* **61**, 4385 (1987); P. P. Freitas, A. A. Gomes, T. R. McGuire, and T. S. Plaskett, J. Magn. Magn. Mater. **83**, 113 (1990).

[32] G. Simmons and H. Wang, *Single Crystal Elastic Constants and Calculated Aggregate Properties: A Handbook*, 2nd ed. (The MIT Press, Cambridge, 1971).